

Article

Anion–Cation Recognition Pattern, Thermal Stability and DFT-Calculations in the Crystal Structure of $H_2dap[Cd(HEDTA)(H_2O)]$ Salt ($H_2dap = H_2(N_3,N_7)$ -2,6-Diaminopurinium Cation)

Jeannette Carolina Belmont-Sánchez¹, Noelia Ruiz-González¹, Antonio Frontera² , Antonio Matilla-Hernández¹ , Alfonso Castiñeiras³ and Juan Niclós-Gutiérrez^{1,*}

¹ Department of Inorganic Chemistry, Faculty of Pharmacy, University of Granada, 18071 Granada, Spain; carol.bs.quimic@hotmail.com (J.C.B.-S.); noeliarg13@correo.ugr.es (N.R.-G.); amatilla@ugr.es (A.M.-H.)

² Departament de Química, Universitat de les Illes Balears, Crta. de Valldemossa km 7.5, 07122 Palma de Mallorca (Balears), Spain; toni.frontera@uib.es

³ Department of Inorganic Chemistry, Faculty of Pharmacy, University of Santiago de Compostela, 15782 Santiago de Compostela, Spain; alfonso.castineiras@usc.es

* Correspondence: jniclos@ugr.es

Received: 24 March 2020; Accepted: 14 April 2020; Published: 15 April 2020



Abstract: The proton transfer between equimolar amounts of $[Cd(H_2EDTA)(H_2O)]$ and 2,6-diaminopurine (Hdap) yielded crystals of the out-of-sphere metal complex $H_2(N_3,N_7)dap [Cd(HEDTA)(H_2O)] \cdot H_2O$ (1) that was studied by single-crystal X-ray diffraction, thermogravimetry, FT-IR spectroscopy, density functional theory (DFT) and quantum theory of “atoms-in-molecules” (QTAIM) methods. The crystal was mainly dominated by H-bonds, favored by the observed tautomer of the 2,6-diaminopurinium(1+) cation. Each chelate anion was H-bonded to three neighboring cations; two of them were also connected by a symmetry-related anti-parallel π, π -stacking interaction. Our results are in clear contrast with that previously reported for $H_2(N_1,N_9)ade [Cu(HEDTA)(H_2O)] \cdot 2H_2O$ (EGOWIG in Cambridge Structural Database (CSD), Hade = adenine), in which H-bonds and π, π -stacking played relevant roles in the anion–cation interaction and the recognition between two pairs of ions, respectively. Factors contributing in such remarkable differences are discussed on the basis of the additional presence of the exocyclic 2-amino group in 2,6-diaminopurinium(1+) ion.

Keywords: EDTA; 2,6-diaminopurine; cadmium; co-crystal; H-bonding; π – π stacking

1. Introduction

Nucleobase complexes with transition metals are continuously under investigation due to their applications as advanced functional materials, their biologic importance, structural diversity and use as molecular recognition models for nucleic acids [1–6]. The majority of structural information available in these systems is mainly dedicated to the adenine nucleobase [7–16] and a variety of N-alkylated derivatives as ligands [17–31]. In contrast, available structural information in the Cambridge Structural Database (CSD) on metal complexes, co-crystals and salts with 2,6-diaminopurine (Hdap) nucleobase is much more limited, despite the fact that Hdap is an analog of adenine. Interestingly, the Hdap nucleobase is able to form the same coordination bonds than adenine and, additionally, the extra exocyclic amino group of Hdap can further function as H-bond donor. Therefore, Hdap can generate novel metal complexes, coordination polymers and supramolecular assemblies.

This study reports the synthesis, X-ray structure and density functional theory study of a new metal complex of formula $H_2(N_3,N_7)dap[Cd(HEDTA)(H_2O)] \cdot H_2O$ (1). A comparison with the previously

reported analog of adenine, $[\text{Cu}(\text{HEDTA})(\text{H}_2\text{O})]\cdot 2\text{H}_2\text{O}$ [5,32], was also performed. The H-bonding networks that are established at both faces of H_2dap were also studied using DFT calculations and the relative strength of each H-bond was estimated using the QTAIM theory. The antiparallel π,π -stacking interactions that were formed between the cations were also studied, focusing on the effect of the counter-ions.

2. Materials and Methods

2.1. Reagents

H_4EDTA acid (TCI), Hdap (Alfa Aesar) and CdCO_3 (Alfa Aesar) were used as received.

2.2. Crystallography

A colorless needle crystal of $\text{H}_2\text{dap}[\text{Cd}(\text{HEDTA})(\text{H}_2\text{O})]\cdot \text{H}_2\text{O}$ (**1**) was mounted on a glass fiber and used for data collection. Crystal data were collected at 100(2) K, using a Bruker D8 VENTURE PHOTON III-14 diffractometer. Graphite-monochromated $\text{MoK}(\alpha)$ radiation ($\lambda = 0.71073 \text{ \AA}$) was used throughout. The data were processed with APEX2 [33] and corrected for absorption using SADABS (transmissions factors: 1.000–0.962) [34]. The structure was solved by direct methods using the program SHELXS-2013 [35] and refined by full-matrix least-squares techniques against F^2 using SHELXL-2013 [35]. Positional and anisotropic atomic displacement parameters were refined for all non-hydrogen atoms. Hydrogen atoms were located in difference maps and included as fixed contributions riding on attached atoms with isotropic thermal parameters 1.2/1.5 times those of their carrier atoms. Criteria of a satisfactory complete analysis were the ratios of 'rms' shift to standard deviation less than 0.001 and no significant features in final difference maps. Atomic scattering factors were taken from the International Tables for Crystallography [36]. Molecular graphics were plotted with PLATON [37]. A summary of the crystal data, experimental details and refinement results are listed in Table 1. Crystallographic data for **1** has been deposited in the Cambridge Crystallographic Data Center with the CCDC number 1992206.

2.3. Other Physical Measurements

Analytical data (CHN) were obtained in a Fisons–Carlo Erba EA 1108 elemental micro-analyzer. The cadmium content was checked as CdO by the weight of final residue in the thermogravimetric analysis (TGA) within 1% of assumed experimental error. FT-IR spectrum was recorded (KBr pellet) on a Jasco FT-IR 6300 spectrometer. TGA was carried out (r.t. to $950 \text{ }^\circ\text{C}$) in air flow (100 mL/min) by a Shimadzu Thermobalance TGA–DTG–50H instrument and a series of 35 time-spaced FT-IR spectra of evolved gasses were recorded with a coupled FT-IR Nicolet Magna 550 spectrometer.

2.4. Synthesis and Relevant IR Spectrum Data

Compound **1** was obtained in a two-step process. First, CdCO_3 (1 mmol, 0.17 g) and H_4EDTA (1 mmol, 0.29 g) were reacted in water (100 mL) inside an open Kitasato flask at $50\text{--}70 \text{ }^\circ\text{C}$, with permanent stirring until a clear solution was observed. The heat was ceased and then small portions of Hdap (1 mmol, 0.15 g) were added to the $\text{Cd-H}_2\text{EDTA}$ chelate. The reaction mixture was filtered without vacuum (to remove any insoluble material) on a crystallization flask. The slow evaporation of the solution (two-three weeks at r.t.) produces needle crystals of **1**. Yield: ~70%. Elemental analysis (%): Calc. for $\text{C}_{15}\text{H}_{24}\text{CdN}_8\text{O}_{10}$: C 30.60, H 4.11, N 19.03, Cd (as CdO) 21.81; Found: C 30.57, H 4.08, N 18.87, Cd (as CdO , final residue at $675 \text{ }^\circ\text{C}$, in the TGA curve) 22.46. FT-IR data [cm^{-1}]: 3500–3100 vbr $\nu_{\text{as}}/\nu_{\text{s}}(\text{H}_2\text{O}) + \nu_{\text{as}}/\nu_{\text{s}}(\text{NH}_2) + \nu_{\text{as}}(\text{NH})$, 3411s, br, $\nu(\text{OH})$, 2931w $\nu_{\text{as}}(\text{CH}_2)$, 1674s, $\nu(\text{C}=\text{O})$, 1596 vs $\delta(\text{NH}_2) + \delta(\text{H}_2\text{O}) + \nu_{\text{as}}(\text{COO})$, 1400 m $\nu_{\text{s}}(\text{COO})$, 923 w, 849 w $\pi(\text{C-H})$.

Table 1. Crystal data and structure refinement for H₂(N₃,N₇)dap[Cd(HEDTA)(H₂O)]·H₂O.

Empirical Formula	C ₁₅ H ₂₄ CdN ₈ O ₁₀
Formula weight	588.82
Temperature	100(2) K
Wavelength	0.71073 Å
Crystal system, space group	Triclinic, P-1
Unit cell dimensions	a = 7.4924(3) Å, α = 81.9310(10)° b = 9.0078(4) Å, β = 78.0170(10)° c = 17.2884(6) Å, γ = 70.545(2)°
Volume	1072.99(8) Å ³
Z, Calculated density	2, 1.822 Mg/m ³
Absorption coefficient	1.090 mm ⁻¹
F(000)	596
Crystal size	0.160 × 0.030 × 0.020 mm
Theta range for data collection	2.405 to 30.507°
Limiting indices	−10 ≤ h ≤ 10, −12 ≤ k ≤ 12, −24 ≤ l ≤ 24
Reflections collected / unique	88812 / 6551 [R(int) = 0.0556]
Completeness to θ = 25.242	99.9%
Absorption correction	Semi-empirical from equivalents
Max. and min. transmission	1.000 and 0.962
Refinement method	Full-matrix least-squares on F ²
Data / restraints / parameters	6551 / 0 / 307
Goodness-of-fit on F ²	1.073
Final R indices [I > 2σ(I)]	R ₁ = 0.0222, wR ₂ = 0.0454
R indices (all data)	R ₁ = 0.0273, wR ₂ = 0.0477
Largest diff. peak and hole	0.588 and −0.469 e.Å ⁻³
CCSD refcode	1992206

2.5. Theoretical Methods

All DFT calculations were carried out using the Gaussian-16 program [38] at the PBE1PBE-D3/def2-TZVP level of theory and using the crystallographic coordinates. The formation energies of the assemblies have been evaluated by calculating the difference between the total energy of the assembly and the sum of the monomers that constitute the assembly, which have been maintained frozen. This methodology has been used by us [39,40] and others [41–45] to analyze supramolecular assemblies in crystal structures. The molecular electrostatic potential was computed at the same level of theory and plotted onto the 0.001 a.u. isosurface. The quantum theory of atoms-in-molecules (QTAIM) [46] analysis was carried out at the same level of theory by means of the AIMAll program [47]. The Cartesian coordinates of the theoretical models are given in the Supplementary Materials.

3. Results and Discussion

3.1. Thermal Stability

Under air-dry flow, the weight loss versus temperature TGA behavior consists of five steps (Figure 1). The experimental results and assignments are summarized in Table 2.

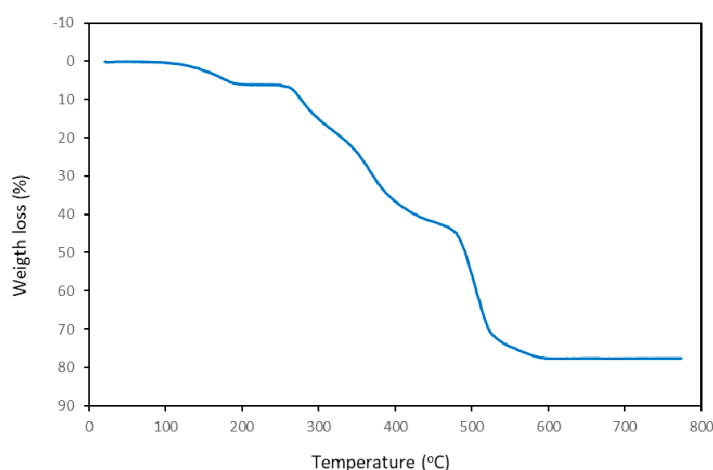


Figure 1. Weight loss versus temperature (in the range r.t. to 775 °C) in the thermogravimetric analysis of compound 1 (sample: 12.29 mg).

Table 2. Summary of the results and assignments in the thermogravimetric analysis of compound 1.

Step or R	Temperature (°C)	Time (min)	Weight (%)		Evolved Gases or Residue (R)
			Experimental	Calculated	
1	55–220	2.5–21	6.056	6.159 *	2 H ₂ O, CO ₂ (t)
2	220–315	21–31	12.071	-	CO ₂ , H ₂ O, CO,
3	315–450	31–43	23.569	-	CO ₂ , H ₂ O, CO, NH ₃ , N ₂ O, NO, NO ₂ , CH ₄
4	450–560	43–53	33.071	-	CO ₂ , H ₂ O, CO, NH ₃ , N ₂ O, NO, NO ₂ , CH ₄
5	560–600	53–70	2.676	-	CO ₂ , H ₂ O, NH ₃ , N ₂ O, NO, NO ₂
R	600	-	22.557	21.808	CdO
R	675	-	22.462	21.808	CdO

* Calculated only for the loss of 2 H₂O. t = trace amounts.

First of all, compound 1 overlaps the loss of uncoordinated water and aqua ligand content (with small amounts of CO₂) in a consistent wide range of temperature (55–220 °C, experimental lost 6.056%, calculated for 2 H₂O molecules 6.159%). In the second step (200–315 °C, with a weight loss of 12.071%) only CO₂, CO and H₂O were evolved, strongly suggesting that the combustion of organic ligands begins by the HEDTA³⁻ chelator. Third and fourth steps (315–450 and 450–560 °C) produce (in addition to H₂O, CO₂ and CO) NH₃ and N-oxides (N₂O, NO and NO₂) plus amounts of CH₄. In the last fifth step (560–675 °C) the presence of CH₄ and CO were less relevant. The weight loss during the burning steps (under an air flow) of organic material cannot be attributed to specific fragments of HEDTA³⁻ or H₂dap⁺. In contrast, the estimated residue (22.557% at 600 °C and 22.462% at 675 °C) reasonably agrees to the calculated weight for CdO (21.808%) within a reasonable experimental error (<1%).

3.2. Crystal Structure and Anion–Cation Recognition Pattern

This compound has an equimolar ratio of the tautomer H₂(N3,N7)dap⁺ cation, the ternary anion [Cd(HEDTA)(H₂O)]⁻ and an unbounded to the metal aqua molecule (Figure 2). Table 3 shows the coordination bond distances and angles in the novel Cd(II) ‘out-sphere’ complex. Table 4 reports data concerning H-bonding interactions in its crystal. The first structural insight was that the assumed most basic N9 donor atom of Hdap diamino–purine in such a tautomeric form of the cation was unable to remove the aqua ligand from the seven coordinated Cd(II) chelate anion. The [Kr]4d¹⁰ electronic configuration and the size of the Cd(II) center enables its rather common hepta-coordination as well as the inequality of its bond distances [2.267(1)–2.459(1) Å]. The Cd(II) coordination polyhedron in the chelate anions is best referred as a distorted mono-capped octahedron. The shortest bond is Cd–O(aqua) whereas the largest ones (<2.40 Å) were Cd–N10<Cd–O(carboxyl)<Cd–N20. Interestingly the largest

Cd-N20 bond involves de N20-HEDTA atom supporting the N-(carboxymethyl) arm of the chelating ligand. Table 3 summarizes the H-bonding interactions in compound 1.

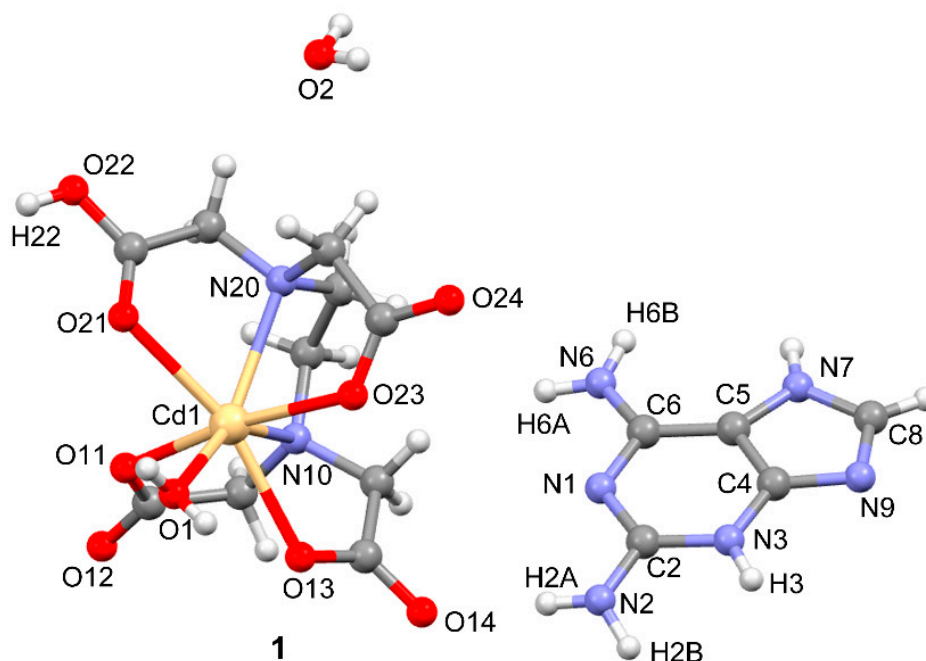


Figure 2. Asymmetric unit in the crystal of compound 1, with relevant atom numbering scheme.

Table 3. Coordination bond lengths (Å) and angles (°) in the crystal of compound 1, H₂(N3,N7) dap[Cd(HEDTA)(H₂O)]·H₂O. See Figure 1 for numbering scheme.

Atoms	Distance or Angle	Atoms	Distance or Angle
Cd(1)-O(1)	2.2672(11)	Cd(1)-N(10)	2.4111(13)
Cd(1)-O(11)	2.2984(11)	Cd(1)-O(21)	2.4400(11)
Cd(1)-O(23)	2.3010(11)	Cd(1)-N(20)	2.4585(13)
Cd(1)-O(13)	2.3748(11)	O(1)-Cd(1)-O(11)	94.13(4)
O(1)-Cd(1)-O(23)	91.28(4)	O(11)-Cd(1)-O(21)	81.61(4)
O(11)-Cd(1)-O(23)	168.52(4)	O(23)-Cd(1)-O(21)	109.06(4)
O(1)-Cd(1)-O(13)	79.59(4)	O(13)-Cd(1)-O(21)	161.48(4)
O(11)-Cd(1)-O(13)	91.09(4)	N(10)-Cd(1)-O(21)	123.95(4)
O(23)-Cd(1)-O(13)	79.93(4)	O(1)-Cd(1)-N(20)	138.89(4)
O(1)-Cd(1)-N(10)	145.66(4)	O(11)-Cd(1)-N(20)	111.24(4)
O(11)-Cd(1)-N(10)	73.31(4)	O(23)-Cd(1)-N(20)	70.22(4)
O(23)-Cd(1)-N(10)	96.63(4)	O(13)-Cd(1)-N(20)	129.28(4)
O(13)-Cd(1)-N(10)	69.10(4)	N(10)-Cd(1)-N(20)	74.65(4)
O(1)-Cd(1)-O(21)	83.96(4)	O(21)-Cd(1)-N(20)	69.17(4)

In the crystal, each anion is H-bonded to three independent neighboring cations, revealing that the anion–cation recognition of 1 is mainly featured by this kind of inter-molecular interaction (Figure 3). Deeping in this question, a H₂dap⁺ cation links the complex anions by the H-bonds: N2-H2B...O24#1 (2.987(1) Å, 169.5°), N3-H3...O23#1 (2.712(1) Å, 179.5°) and (aqua)O1-H1WA...N9#1 (2.902(1) Å, 166.6°) with #1 = -x + 1, -y + 1, -z + 1. This recognition pattern involves both O-acceptors of the same HEDTA⁻ carboxylate group and the most basic N9 atom of the purinium(1+) ion. Another H₂dap ion builds two H-bonds with O-carboxylate acceptors of the same HEDTA⁻ carboxylate group: N6-H6B...O13#5 (2.831(1) Å, 1.67.7°) and N7-H7...O14#5 (2.675(1) Å, 177.2°) with #5 = x, -y, z. Figure 4 shows the way these two purinium(1+) cations were additionally related by a moderate anti-parallel π,π-stacking interaction between their 5- and 6-membered rings (inter-centroid distance d_{c-c} 3.49 Å, interplanar

distance $d_{\pi-\pi}$ 3.21 Å, dihedral interplanar angle 0° , slipping angles $\beta = \gamma = 25.91^\circ$, slippage index 1.56). In this interaction the shortest interplanar distance would be related to the remarkable slippage. A third purinium(1+) ion is related with the chelate anion by the H-bond N6-H6A...O24 (2.990(1) Å, 144.6°). Thus, O24 atom acts as twice-acceptor for H-bonding interactions.

Table 4. Geometric features of the hydrogen bonds in the crystal structure of $H_2(N3,N7)dap [Cd(HEDTA)(H_2O)] \cdot H_2O$ (1). The distances were measured between the heavy atoms.

H-bond	D...A (Å)	Angle ($^\circ$)
O(1)-H(1WA)...N(9)#1	2.9017(17)	166.6
O(1)-H(1WB)...O(12)#2	2.7398(16)	169.0
O(22)-H(22)...O(11)#3	2.5552(16)	175.5
N(2)-H(2A)...O(14)	2.8158(18)	165.9
N(2)-H(2B)...O(24)#1	2.9784(18)	169.5
N(3)-H(3)...O(23)#1	2.7123(17)	179.5
N(6)-H(6A)...O(24)#4	2.9898(18)	144.6
N(6)-H(6B)...O(13)#5	2.8307(17)	167.7
N(7)-H(7)...O(14)#5	2.6746(18)	177.2
O(2)-H(2WA)...O(12)#6	2.7517(17)	163.4
O(2)-H(2WB)...O(11)#7	2.9970(18)	131.5

Symmetry transformations to generate equivalent atoms: #1 $-x + 1, -y + 1, -z + 1$, #2 $x + 1, y, z$, #3 $-x + 1, -y + 2, -z$, #4 $x - 1, y, z$, #5 $x, y - 1, z$, #6 $x + 1, y - 1, z$, #7 $-x + 1, -y + 1, -z$.

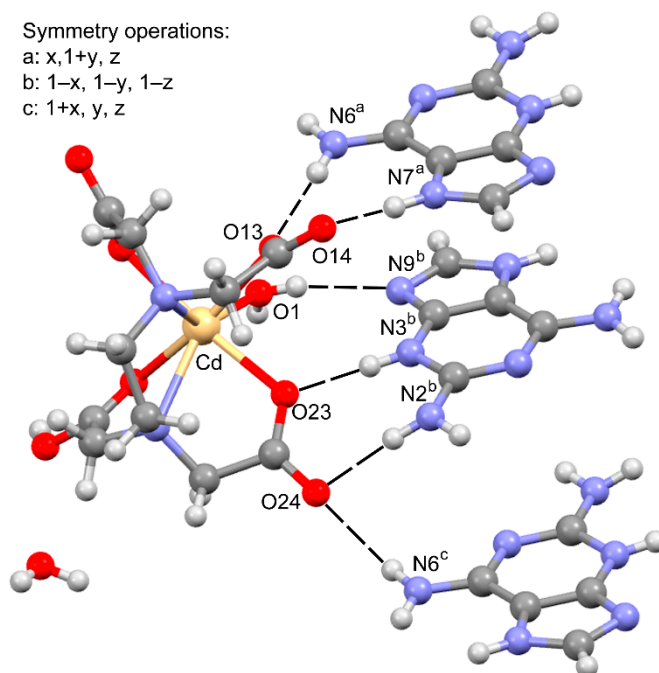


Figure 3. Molecular recognition pattern showing the cooperation of H-bonds between the $[Cd(HEDTA)(H_2O)]^-$ chelate anion and three neighboring $H_2(N3,N7)dap^+$ ions.

In this compound all N–H and O–H bonds were involved in N–H...O or O–H...O interactions excepting for the above mentioned (aqua)O(1)-H(1WA)...N(9)#1 one (Table 3). In this manner the packing was essentially dominated by the H-bonding array that forms bilayers with Cd(II) chelate anions and unboned water molecules whereas $H_2(N3,N7)dap^+$ ions fall oriented towards both external surfaces. These 2D-frameworks lie parallel to the ab crystal plane and were H-bonded pillared along the c axis in the 3D-network (Figure 5).

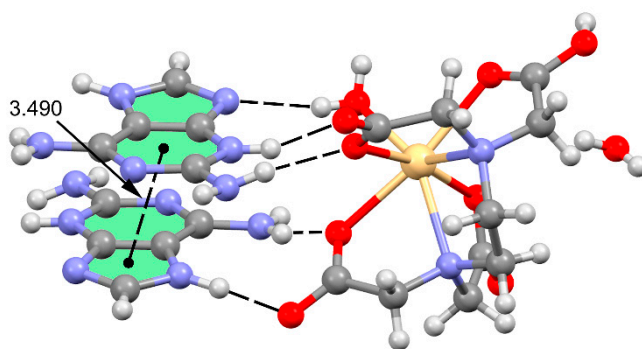


Figure 4. Molecular recognition pattern showing the cooperation of H-bonds and π,π -stacking interactions connecting the $[\text{Cd}(\text{HEDTA})(\text{H}_2\text{O})]^-$ chelate anion with two of the neighboring $\text{H}_2(\text{N}3,\text{N}7)\text{dap}^+$ ions.

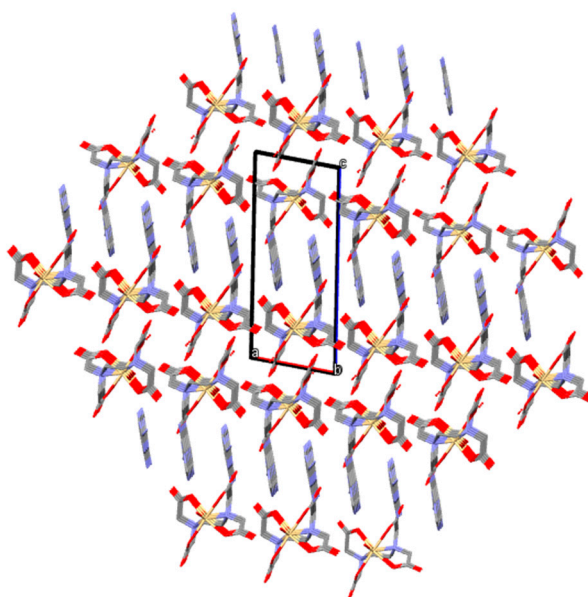


Figure 5. In the 3D H-bonded crystal of compound **1**, 2,6-diaminopurinium(1+) cations oriented towards the external faces of 2D H-bonded frameworks build by complex anions and unbounded to the cadmium(II) water molecules. All H atoms and H-bonding interactions are omitted for clarity.

3.3. DFT Calculations

The DFT study was focused to analyze the interesting supramolecular assemblies and H-bonding networks described above. First of all, the molecular electrostatic potential (MEP) surfaces of the anion and cation have been calculated in order to evaluate the best complementary dimer in terms of the electrostatic attraction between electron rich and electron poor regions of both molecules. The pure Coulombic attraction between the counter-ions is not directional; however weaker interaction like H-bonds or π,π -stacking interactions were able to nicely tune the final geometry of the supramolecular assembly. Evidence for the possibly structure-directing nature of these contacts was supported through an examination of MEP surfaces represented in Figure 6a. These reveal strong electropositive region (blue) at the NH groups of the Hdap^+ cation and at the H-atoms of the Cd-coordinated water molecule. Moreover, the surfaces show excess of negative charge (red) at the O-atoms of the Cd-coordinated carboxylate group and at the N-atom of the five-membered ring of H_2dap^+ thus affording potentially favorable O-H \cdots N and N-H \cdots O interactions between the counter-ions. The MEP surface of Hdap^+ also evidences that the N1-atom was less basic than N9, thus it was a worse H-bond acceptor. The MEP surface of the complex represented in Figure 6b shows how the charge density was significantly redistributed upon complexation.

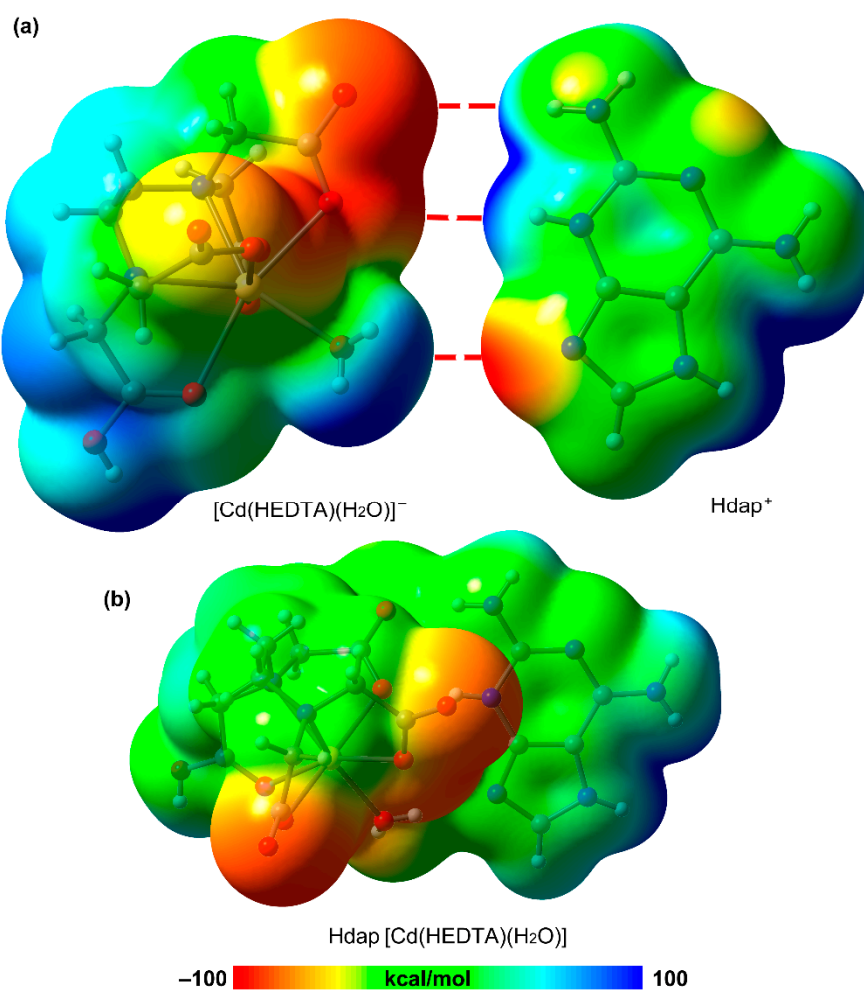


Figure 6. (a) MEP surfaces (0.001 a.u.) for $[\text{Cd}(\text{HEDTA})(\text{H}_2\text{O})]^-$ and H_2dap^+ highlighting the electropositive (blue) and electronegative (red) regions of each molecule. The dashed lines highlight a favorable electrostatic interaction between these two species. (b) MEP surface (0.001 a.u.) of the assembly at the PBE1PBE/def2-TZVP level of theory.

We have selected the supramolecular assembly commented above in Figure 7a–d to analyze the energetic features of the H-bonds and π,π -stacking interactions in **1**. Figure 7a shows a partial view of the solid state of **1** where these interactions are highlighted. From this quaternary assembly, we have first analyzed two H-bonded dimers (see Figure 7b,c), which present very large dimerization energies due to the strong contribution of the electrostatic attraction between counter-ions. Curiously the dimer with two H-bonds (Figure 7c) was stronger than that with three H-bonds (Figure 7b), likely due to the shorter H-bond distances. This aspect is further analyzed below. Regarding the π,π -stacked dimer, it presents a positive (repulsive) binding energy because it occurs against the Coulombic repulsion between both H_2dap^+ cations ($\Delta E_3 = +44.8$ kcal/mol). However, if the counter-ions were taken into consideration, the interaction becomes favorable, $\Delta E_4 = -92.8$ kcal/mol.

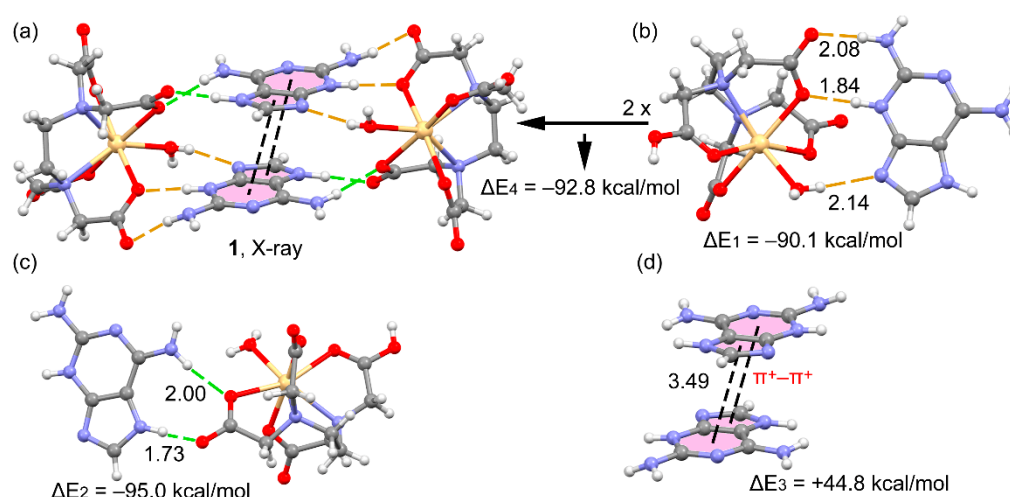


Figure 7. (a) Partial view of the X-ray solid state of **1** showing the self-assembled tetramer. (b,c) H-bonded dimers extracted from the assembly dimers. (d) Isolated π,π -stacked dimer of H2dap⁺ moieties. The distances are given in Å.

As commented above, the interaction energies were strongly dominated by the Coulombic attraction between the counter-ions and it was difficult to evaluate the real effect of the H-bonding interactions. In order to better analyze the H-bonding network, we have used the QTAIM method to estimate the contribution of each H-bond. The existence of a bond path (lines of maximum density) and bond critical point (CP) connecting two atoms is a universal indication of interaction [48]. The distribution of bond CPs and bond paths in the two H-bonded dimers of compound **1** are given in Figure 8. Each H-bond interaction was characterized by a bond CP (green sphere) and bond path interconnecting the H-atom to the N/O-atoms and confirming the interaction. The energy of each contact has been evaluated according to the approach suggested by Espinosa et al. [49] and Vener et al. [50]. The energy predictors were developed specifically for HBs and were based on the kinetic energy density (V_r) of the Lagrangian energy density (G_r). These values along with the charge density (ρ_r) are summarized in Table 5 for the CPs indicated in Figure 8. It can be observed that both energy predictors show that the N9-H...O H-bond (CP4) was the strongest one, even stronger than N3⁺-H3...O (the second strongest HB) that bears the positive charge, in line with the shortest distance (1.73 Å) and larger electron density (ρ_r) of CP4, see Table 5. The dissociation energies obtained for the other H-bonds were in the typical range of moderately strong H-bonds. There is an acceptable agreement between both energy predictors thus giving reliability to the study. It is worth mentioning that the sum of the dissociation energies of the two H-bonds of the dimer shown in Figure 8b (18.62 kcal/mol, using the V_r predictor) was larger than the sum of the three H-bonds in the dimer shown in Figure 8a (16.60 kcal/mol), in good agreement with the DFT energies computed for the assemblies shown in Figure 7a,b. This result confirms the fact that the H-bonds were stronger in the dimer where only two H-bonds were formed. Finally, it is interesting to note that the total energy density ($H_r = V_r + G_r$) was negative in CP4 thus evidencing partial covalent character for the N9-H9...O H-bond, in agreement with its large dissociation energy. The rest of CPs exhibit positive H_r values, evidencing their negligible covalent character.

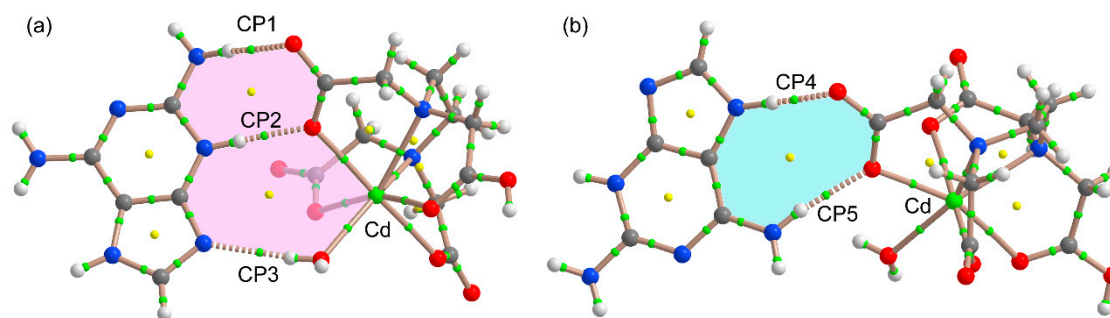


Figure 8. (a,b). Distribution of bond and ring critical points (green and yellow spheres, respectively) and bond paths in two dimers of complex 1. The QTAIM data at the bond CPs denoted as CP1 to CP5 are given in Table 3.

Table 5. Values of ρ_r , V_r and G_r (in a.u.) for CP1 to CP5 as indicated in Figure 7. The dissociation energy (E_{dis}) of each H-bond based on V_r and G_r parameters are also indicated in kcal/mol.

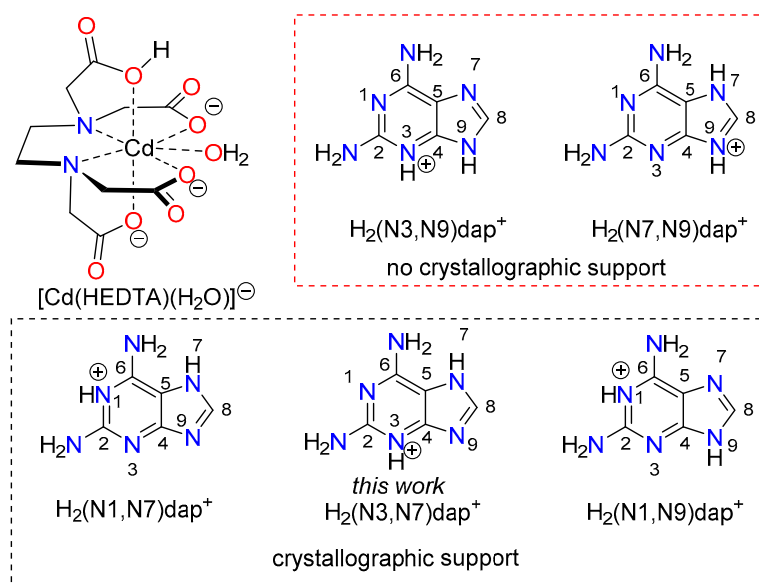
CP#	ρ_r	V_r	G_r	$E_{dis} (-0.5 \times V_r)$	$E_{dis} (0.429 \times G_r)$
1	0.0186	-0.0122	0.0155	3.83	4.17
2	0.0328	-0.0297	0.0308	9.32	8.29
3	0.0171	-0.0110	0.0148	3.45	3.98
4	0.0429	-0.0421	0.0380	12.2	10.2
5	0.0224	-0.0172	0.0207	6.49	5.57

3.4. Structural Insides on N(heterocyclic)-Proton Affinities, H-Tautomerism and Metal Binding Patterns from Hdap and Its Cationic Forms in Salts and Their Metal Complexes.

In a rather comprehensive review [51] we have look at the molecular recognition patterns between metal complexes and adenine or a variety of deaza- and aza-adenines (such as Hdap) on the basis of the cooperation between coordination bonds and intra-molecular interligand H-bonding interactions. This review emphasizes the relevance of the N(heterocyclic)-H tautomeric possibilities in neutral and protonated forms of such kinds of natural or synthetic closely related N-heterocyclic ligands. Recent reports from our groups extend these points of view to the guanine-synthetic acyclovir as a ligand [52–54]. Now we have the opportunity to deep into the relevance of these factors on the basis of the available crystallographic results related to cationic forms of Hdap, its salts and inner- or out-sphere metal complexes.

It is generally assumed that the proton affinity of hardly versatile ligand adenine (Hade) follows the order $N9 > N1 > N7 > N3 > N6$ (exocyclic amino) [51]. In a private communication to the CSD basis [55] the structure of the salt $H_3(N1, N7, N9)dapCl_2 \cdot H_2O$ (see reference code NULCOO in CSD Database) revealed the lesser proton affinity of the N3 atom of Hdap. That seems also agree with the depleted proton affinity found for the N3-atom of acyclovir, a well-known guanine-synthetic nucleoside [52]. The tautomers $H_2(N1, N3)dap^+$, $H_2(N3, N9)dap^+$ and $H_2(N7, N9)dap^+$ do not have received crystallographic support. The $H_2(N1, N7)dap^+$ tautomer acts as N9-donor ligand in two isomorphous compounds having all-trans octahedral complex molecules $[M^{II}(H_2dap)_2(hpt)_2(H_2O)_2] \cdot 4H_2O$ ($M = Co$ or Ni , $hpt =$ homophthalato(2-) ligand) [56] (see Scheme 1). The $\kappa N9-H_2(N1, N7)dap^+$ coordinating role was consistent not only with the highest proton affinity of the donor atom but also to its less steric hindrance. Interestingly in these complexes there was a cooperation of each M-N9 bond with an intra-molecular (aqua)O-H...N3 interligand interaction. The $H_2(N1, N9)dap^+$ tautomer was the counter cation of two rather distinct salts, with a dicarboxylate [57] or a dodecafluoro-*closo*-dodecaborate(2-) anion [58]. This tautomer binds metal ions by its N7-donor, in two Cd(II)-dicarboxylate coordination polymers [59,60] and a mononuclear Co(II) complex [61] displaying the appropriate cooperation between the metal-N7 coordination bond and an N6-H...O interligand interaction. This tautomeric

form was in agreement of the N-proton affinity assumed for the free base Hdap (N9>N1>N7>N3) which is also consistent by the crystal structure of H(N9)dap·H₂O [59].



Scheme 1. Structure of $[\text{Cd}(\text{HEDTA})(\text{H}_2\text{O})]^-$ and different tautomeric forms of Hdap^+ with the atom numbering scheme.

The $\text{H}_2(\text{N3},\text{N7})\text{dap}^+$ tautomer, also here reported, is previously document in three rather distinct compounds. The out-sphere complex $(\text{H}_2(\text{N3},\text{N7})\text{dap})_2[\text{Nd}(\mu_2\text{-croco})(\text{croco})(\text{H}_2\text{O})_4]_2$ (croco = croconate(2-) ion). This compound also builds a sophisticated H-bonded network, carefully describe by R. Baggio et al. [62] where any relevant π,π -stacking interactions appears precluded by coordination of the croco ligands. Why the $\text{H}_2(\text{N3},\text{N7})\text{dap}^+$ ions does not bind to Nd(III) centers can be explained on the basis of the Pearson's border-line basis of the Hdap and its cation whereas trivalent lanthanide cations were typical hard Pearson's acids. The two other compounds exhibit the $\kappa\text{N9-H}_2(\text{N3},\text{N7})\text{dap}^+$ ligand mode in presence of benzene-polycarboxylate anions. In the complex cation of $\text{trans-}[\text{Co}^{\text{II}}(\text{H}_2\text{O})_4(\text{H}_2(\text{N3},\text{N7})\text{dap})_2](\text{btc})\cdot 4\text{H}_2\text{O}$ (btc = benzene-1,2,4,5-tetracarboxylate) [63], aqua ligands cannot acts as H-acceptor for the N3-H bond of the $\text{H}_2(\text{N3},\text{N7})\text{dap}^+$ ions. Consequently, the Co-N9[$\text{H}_2(\text{N3},\text{N7})\text{dap}$] coordination bond does not cooperate with an interligand N3-H...O interaction. In clear contrast the polymeric compound $[\{\text{Zn}(\text{btc})(\text{H}_2\text{O})(\text{H}_2(\text{N3},\text{N7})\text{dap})\}\cdot 4\text{H}_2\text{O}]_n$ (btc = benzene-1,2,3-tricarboxylate(3-) ion) exhibits the cooperation between the Zn-N9 coordination bond and an interligand (H_2dap) N3-H...O(carboxy, btc) interaction (2.587(4) Å, 157°) [59]. Curiously the O-carboxylate(btc) acceptor involved in such interligand H-bonding interaction implies an un-bonded to the Zn(II) O atom. This is certainly a relevant fact because of the common cooperation of metal-N(purine-like) bonds with (purine-like)N-H...O(carboxylate) intra-molecular interligand interactions was built with a metal-O(coordinated) H-acceptor atom [53].

4. Concluding Remarks

In summary, the proton transfer between 2,6-diaminopurine and $[\text{Cd}(\text{H}_2\text{EDTA})(\text{H}_2\text{O})]$ yields the outer sphere complex reported herein. The geometric features of the nucleobase in the solid state have been discussed in terms of binding pattern, protonation degree and proton tautomer as well as the hydrogen-bonding. Significantly, the solid-state structure was tuned by the synergistic formation of H-bonds and $\pi^+-\pi^+$ interactions that have been described in detail. Moreover, the interaction energies of several supramolecular assemblies observed in the solid state have been evaluated and discussed by using MEP surfaces and DFT calculations. Finally, the individual H-bonding dissociation energies have been computed using two available energy predictors by means of the QTAIM method.

On the basis of our results and other above referred, it seems clear that the tautomerism plays a relevant role in the crystal having H₂dap⁺ ions. The lack of literature concerning H₂(N1,N3)dap⁺, H₂(N3,N9)dap⁺ and H₂(N7,N9)dap⁺ could be related to one of the following factors: The steric hindrance on N1, the depleted proton affinity of N3 and the suitability of the highest basic of N7 and N9 to metal binding. In the here reported compound, the use of the H₂(N3,N7)dap⁺ favors the extensive H-bonding of its crystal, at the same time that precludes its coordination to the Cd(II) center instead of the aqua ligand.

Supplementary Materials: The following are available online at <http://www.mdpi.com/2073-4352/10/4/304/s1>, Cartesian coordinates of the theoretical models shown in Figure 7.

Author Contributions: Conceptualization, J.N.-G. and A.M.-H.; methodology, all authors; software, A.M.-H., A.F. and A.C.; investigation, J.C.B.-S. and N.R.-G.; writing—original draft preparation, A.M.-H., A.C., A.F. and J.N.-G., writing—review and editing, all authors, visualization, A.M.-H., A.C., A.F. project administration, J.N.-G.; funding acquisition, A.M.-H., A.F. and J.N.-G. All authors have read and agreed to the published version of the manuscript.

Funding: This research was funded by the Excellence Network ‘Metal Ions in Biological Systems’ MetalBio CTQ2017-90802-REDT, the Research group FQM-283 (Junta de Andalucía) and MICIU/AEI of Spain (project CTQ2017-85821-R FEDER funds).

Acknowledgments: We thank the Centre de Tecnologies de la Informació (CTI), Universitat de les Illes Balears for computational facilities. We also thank all projects for financial support.

Conflicts of Interest: The authors declare no conflict of interest.

References

1. Terrón, A.; Fiol, J.J.; García-Raso, A.; Barceló-Oliver, M.; Moreno, V. Biological recognition patterns implicated by the formation and stability of ternary metal ion complexes of low-molecular-weight formed with amino acid/peptides and nucleobases/nucleosides. *Coord. Chem. Rev.* **2007**, *251*, 1973–1986. [[CrossRef](#)]
2. Sivakova, S.; Rowan, S.J. Nucleobases as supramolecular motifs. *Chem. Soc. Rev.* **2005**, *34*, 9–21. [[CrossRef](#)]
3. Lippert, B. Multiplicity of metal ion binding patterns to nucleobases. *Coord. Chem. Rev.* **2000**, *200–202*, 487–516. [[CrossRef](#)]
4. Navarro, J.A.R.; Lippert, B. Simple 1:1 and 1:2 complexes of metal ions with heterocycles as building blocks for discrete molecular as well as polymeric assemblies. *Coord. Chem. Rev.* **2001**, *222*, 219–250. [[CrossRef](#)]
5. Choquesillo-Lazarte, D.; Brandi-Blanco, M.P.; García-Santos, I.; González-Pérez, J.M.; Castiñeiras, A.; Niclós-Gutiérrez, J. Interligand interactions involved in the molecular recognition between copper (II) complexes and adenine or related purines. *Coord. Chem. Rev.* **2008**, *25*, 1241–1256. [[CrossRef](#)]
6. Olea, D.; Alexandre, S.S.; Amo-Ochoa, P.; Guijarro, A.; De Jesus, F.; Soler, J.M.; De Pablo, P.J.; Zamora, F.; Gomez-Herrero, J. From Coordination Polymer Macrocrystals to Nanometric Individual Chains. *Adv. Mater.* **2005**, *17*, 1761–1765. [[CrossRef](#)]
7. García-Terán, J.P.; Castillo, O.; Luque, A.; García-Couceiro, U.; Beobide, G.; Román, P. Molecular Recognition of Adeninium Cations on Anionic Metal–Oxalato Frameworks: An Experimental and Theoretical Analysis. *Inorg. Chem.* **2007**, *46*, 3593–3602. [[CrossRef](#)]
8. González-Pérez, J.M.; Alarcón-Payer, C.; Castiñeiras, A.; Pivetta, T.; Lezama, L.; Choquesillo-Lazarte, D.; Crisponi, G.; Niclós-Gutiérrez, J. A Windmill-Shaped Hexacopper(II) Molecule Built Up by Template Core-Controlled Expansion of Diaquatetrakis(μ₂-adeninato-N3,N9)dycopper(II) with Aqua(oxydiacetato)-copper(II). *Inorg. Chem.* **2006**, *45*, 877–882. [[CrossRef](#)]
9. Amo-Ochoa, P.; Rodríguez-Tapiador, M.I.; Castillo, O.; Olea, D.; Guijarro, A.; Alexandre, S.S.; Gómez-Herrero, J.; Zamora, F. Assembling of Dimeric Entities of Cd(II) with 6-Mercaptopurine to Afford One-Dimensional Coordination Polymers: Synthesis and Scanning Probe Microscopy Characterization. *Inorg. Chem.* **2006**, *45*, 7642–7650. [[CrossRef](#)]
10. García-Terán, J.P.; Castillo, O.; Luque, A.; García-Couceiro, U.; Román, P.; Lloret, F. One-Dimensional Oxalato-Bridged Cu(II), Co(II), and Zn(II) Complexes with Purine and Adenine as Terminal Ligands. *Inorg. Chem.* **2004**, *43*, 5761–5770. [[CrossRef](#)]
11. García-Terán, J.P.; Castillo, O.; Luque, A.; García-Couceiro, U.; Román, P.; Lezama, L. An Unusual 3D Coordination Polymer Based on Bridging Interactions of the Nucleobase Adenine. *Inorg. Chem.* **2004**, *43*, 4549–4551. [[CrossRef](#)]

12. Rojas-González, P.X.; Catiñeiras, A.; González-Pérez, J.M.; Choquesillo-Lazarte, D.; Niclós-Gutiérrez, J. Interligand Interactions Controlling the μ -N7,N9-Metal Bonding of Adenine (AdeH) to the N-Benzyliminodiacetato(2-) Copper(II) Chelate and Promoting the N9 versus N3 Tautomeric Proton Transfer: Molecular and Crystal Structure of $[\text{Cu}_2(\text{NBzIDA})_2(\text{H}_2\text{O})_2(\mu\text{-N7,N9-Ade(N3)H})]\cdot 3\text{H}_2\text{O}$. *Inorg. Chem.* **2002**, *41*, 6190–6192. [[PubMed](#)]
13. García-Terán, J.P.; Castillo, O.; Luque, A.; García-Couceiro, U.; Beobide, G.; Román, P. Supramolecular architectures assembled by the interaction of purine nucleobases with metal-oxalato frameworks. Non-covalent stabilization of the 7H-adenine tautomer in the solid-state. *Dalton Trans* **2006**, 902–911. [[CrossRef](#)]
14. Bugella-Altamirano, E.; Choquesillo-Lazarte, D.; González-Pérez, J.M.; Sánchez-Moreno, M.J.; Martín-Ramos, R.; Covelo, B.; Carballo, R.; Castiñeiras, A.; Niclós-Gutiérrez, J. Three new modes of adenine-copper(II) coordination: Interligand interactions controlling the selective N3-, N7- and bridging μ -N3,N7-metal-bonding of adenine to different N-substituted iminodiacetato-copper(II) chelates. *Inorg. Chim. Acta* **2002**, *339*, 160–170. [[CrossRef](#)]
15. Suzuki, T.; Hirai, Y.; Monjushiro, H.; Kaizaki, S. Cobalt(III) Complexes of Monodentate N(9)-Bound Adeninate (ade-), $[\text{Co}(\text{ade-}\kappa\text{N9})\text{Cl}(\text{en})_2]^+$ (en = 1,2-Diaminoethane): Syntheses, Crystal Structures, and Protonation Behaviors of the Geometrical Isomers. *Inorg. Chem.* **2004**, *43*, 6435–6444. [[CrossRef](#)]
16. Yang, E.-C.; Zhao, H.-K.; Feng, Y.; Zhao, X.-J. A Tetranuclear Cu^{II} -Based 2D Aggregate with an Unprecedented Tetradentate μ_4 -N1,N3,N7,N9-Adeninate Nucleobase. *Inorg. Chem.* **2009**, *48*, 3511–3513. [[CrossRef](#)]
17. García-Raso, A.; Terrón, A.; Ortega-Castro, J.; Barceló-Oliver, M.; Lorenzo, J.; Rodríguez-Calado, S.; Franconetti, A.; Frontera, A.; Vázquez-López, E.M.; Fiol, J.J. Iridium(III) coordination of N(6) modified adenine derivatives with aminoacid chains. *J. Inorg. Biochem.* **2020**, *205*, 111000. [[CrossRef](#)]
18. Ruiz-González, N.; García-Rubiño, M.E.; Domínguez-Martín, A.; Choquesillo-Lazarte, D.; Franconetti, A.; Frontera, A.; Castiñeiras, A.; González-Pérez, J.M.; Niclós-Gutiérrez, J. Molecular and supramolecular recognition patterns in ternary copper(II) or zinc(II) complexes with selected rigid-planar chelators and a synthetic adenine-nucleoside. *J. Inorg. Biochem.* **2020**, *203*, 110920. [[CrossRef](#)]
19. Martínez, D.; Pérez, A.; Cañellas, S.; Silió, I.; Lancho, A.; García-Raso, A.; Fiol, J.J.; Terrón, A.; Barceló-Oliver, M.; Ortega-Castro, J.; et al. Synthesis, reactivity, X-ray characterization and docking studies of N7/N9-(2-pyrimidyl)-adenine derivatives. *J. Inorg. Biochem.* **2020**, *203*, 110879. [[CrossRef](#)]
20. Roitzsch, M.; Lippert, B. Metal Coordination and Imine–Amine Hydrogen Bonding as the Source of Strongly Shifted Adenine pK_a Values. *J. Am. Chem. Soc.* **2004**, *126*, 2421–2424. [[CrossRef](#)]
21. Añorbe, M.G.; Welzel, T.; Lippert, B. Migration of a cis-(NH₃)₂PtII Moiety along Two Adenine Nucleobases, from N1 to N6, is Markedly Facilitated by Additional Pt^{II} Entities Coordinated to N7. *Inorg. Chem.* **2007**, *46*, 8222–8227. [[CrossRef](#)]
22. Purohit, C.S.; Verma, S. A Luminescent Silver–Adenine Metallamacrocyclic Quartet. *J. Am. Chem. Soc.* **2006**, *128*, 400–401. [[CrossRef](#)]
23. Purohit, C.S.; Mishra, A.K.; Verma, S. Four-Stranded Coordination Helices Containing Silver–Adenine (Purine) Metallaquartets. *Inorg. Chem.* **2007**, *46*, 8493–8495. [[CrossRef](#)]
24. Purohit, C.S.; Verma, S. Patterned Deposition of a Mixed-Coordination Adenine–Silver Helicate, Containing a π -Stacked Metallacycle, on a Graphite Surface. *J. Am. Chem. Soc.* **2007**, *129*, 3488–3489. [[CrossRef](#)]
25. Shipman, M.A.; Price, C.; Gibson, A.E.; Elsegood, M.R.J.; Clegg, W.; Houlton, A. Monomer, Dimer, Tetramer, Polymer: Structural Diversity in Zinc and Cadmium Complexes of Chelate-Tethered Nucleobases. *Chem. Eur. J.* **2000**, *6*, 4371–4378. [[CrossRef](#)]
26. Kruger, T.; Ruffer, T.; Lang, H.; Wagner, C.; Steinborn, D. Synthesis, Characterization, and Reactivity of $[\text{Li}(\text{N}^6, \text{N}^9\text{-Me}_2\text{Ade-H})]$: A Structurally Characterized Lithiated Adenine. *Inorg. Chem.* **2008**, *47*, 1190–1195. [[CrossRef](#)]
27. Amantia, D.; Price, C.; Shipman, M.A.; Elsegood, M.R.J.; Clegg, W.; Houlton, A. Minor Groove Site Coordination of Adenine by Platinum Group Metal Ions: Effects on Basicity, Base Pairing, and Electronic Structure. *Inorg. Chem.* **2003**, *42*, 3047–3056. [[CrossRef](#)]
28. Zobi, F.; Spingler, B.; Alberto, R. Structure, Reactivity and Solution Behaviour of $[\text{Re}(\text{ser})(7\text{-MeG})(\text{CO})_3]$ and $[\text{Re}(\text{ser})(3\text{-pic})(\text{CO})_3]$: ‘Nucleoside-mimicking’ Complexes Based on the fac- $[\text{Re}(\text{CO})_3]^+$ Moiety. *Dalton Trans.* **2005**, 2859–2865. [[CrossRef](#)]

29. Jiang, Q.; Wu, Z.-Y.; Zhang, Y.-M.; Hotze, A.C.G.; Hannon, M.J.; Guo, Z.-J. Effect of Adenine Moiety on DNA Binding Property of Copper(II)–terpyridine Complexes. *Dalton Trans* **2008**, 3054–3060. [[CrossRef](#)]
30. Price, C.; Horrocks, B.R.; Mayeux, A.; Elsegood, M.R.J.; Clegg, W.; Houlton, A. Self-Complementary Metal Complexes Containing a DNA Base Pair. *Angew. Chem. Int. Ed.* **2002**, *41*, 1047–1049. [[CrossRef](#)]
31. Dobrzynska, D.; Jerzykiewicz, L.B. Adenine Ribbon with Watson–Crick and Hoogsteen Motifs as the ‘Double-Sided Adhesive Tape’ in the Supramolecular Structure of Adenine and Metal Carboxylate. *J. Am. Chem. Soc.* **2004**, *126*, 11118–11119. [[CrossRef](#)]
32. Serrano Padial, E.; Choquesillo-Lazarte, D.; Bugella Altamirano, E.; Castiñeiras, A.; Carballo, R.; Niclós Gutiérrez, J. New Copper(II) Compound having Protonated forms of Ethylenediamine-tetraacetate(4-) ion (EDTA) and Adenine (AdeH): Synthesis, Crystal Structure, Molecular Recognition and Physical Properties of (AdeH₂)[Cu(HEDTA)(H₂O)]·2H₂O. *Polyhedron* **2002**, *21*, 1451–1457. [[CrossRef](#)]
33. Bruker. *APEX3 Software*; v2018.7-2; Bruker AXS Inc.: Madison, WI, USA, 2018.
34. Sheldrick, G.M. *SADABS. Program for Empirical Absorption Correction of Area Detector Data*; University of Goettingen: Goettingen, Germany, 1997.
35. Sheldrick, G.M. A short history of SHELX. *Acta Crystallogr.* **2008**, *64*, 112–122. [[CrossRef](#)]
36. Wilson, A.J.C. *International Tables of Crystallography*; Kluwer Academic Publishers: Dordrecht, The Netherlands, 1995; Volume C.
37. Spek, A.L. PLATON. A multipurpose Crystallographic tool. *Acta Crystallogr.* **2009**, *65*, 148–155.
38. Frisch, M.J.; Trucks, G.W.; Schlegel, H.B.; Scuseria, G.E.; Robb, M.A.; Cheeseman, J.R.; Scalmani, G.; Barone, V.; Petersson, G.A.; Nakatsuji, H.; et al. *Gaussian 16, Revision A.01*; Gaussian, Inc.: Wallingford, CT, USA, 2016.
39. Hazari, A.; Das, L.K.; Kadam, R.M.; Bauza, A.; Frontera, A.; Ghosh, A. Unprecedented structural variations in trinuclear mixed valence Co (II/III) complexes: Theoretical studies, pnictogen bonding interactions and catecholase-like activities. *Dalton Trans.* **2015**, *44*, 3862–3876. [[CrossRef](#)]
40. Mitra, M.; Manna, P.; Bauzá, A.; Ballester, P.; Seth, S.K.; Ray Choudhury, S.; Frontera, A.; Mukhopadhyay, S. 3-Picoline Mediated Self-Assembly of M (II)–Malonate Complexes (M= Ni/Co/Mn/Mg/Zn/Cu) Assisted by Various Weak Forces Involving Lone Pair– π , π – π , and Anion \cdots π –Hole Interactions. *J. Phys. Chem. B* **2014**, *118*, 14713–14726. [[CrossRef](#)]
41. Kolaria, K.; Sahamies, J.; Kalenius, E.; Novikov, A.S.; Kukushkin, V.Y.; Haukka, M. Metallophilic interactions in polymeric group 11 thiols. *Solid State Sci.* **2016**, *60*, 92–98. [[CrossRef](#)]
42. Novikov, A.S.; Ivanov, D.M.; Bikbaeva, Z.M.; Bokach, N.A.; Kukushkin, V.Y. Noncovalent Interactions Involving Iodofluorobenzenes: The Interplay of Halogen Bonding and Weak lp(O) \cdots π -Holearene Interactions. *Cryst. Growth Des.* **2018**, *18*, 7641–7654. [[CrossRef](#)]
43. Kinzhalov, M.A.; Novikov, A.S.; Chernyshev, A.N.; Suslonov, V.V. Intermolecular hydrogen bonding H \cdots Cl– in the solid palladium(II)-diaminocarbene complexes. *Z. Kristallogr. Cryst. Mater.* **2017**, *232*, 299–305. [[CrossRef](#)]
44. Baykov, S.V.; Dabranskaya, U.; Ivanov, D.M.; Novikov, A.S.; Boyarskiy, V.P. Pt/Pd and I/Br Isostructural Exchange Provides Formation of C–I \cdots Pd, C–Br \cdots Pt, and C–Br \cdots Pd Metal-Involving Halogen Bonding. *Cryst. Growth Des.* **2018**, *18*, 5973–5980. [[CrossRef](#)]
45. Usoltsev, A.N.; Adonin, S.A.; Novikov, A.S.; Samsonenko, D.G.; Sokolov, M.N.; Fedina, V.P. One-dimensional polymeric polybromotellurates(IV): Structural and theoretical insights into halogen \cdots halogen contacts. *CrystEngComm* **2017**, *19*, 5934–5939. [[CrossRef](#)]
46. Bader, R.F.W. A quantum theory of molecular structure and its applications. *Chem. Rev.* **1991**, *91*, 893–928. [[CrossRef](#)]
47. Keith, T.A. *AIMAll (Version 13.05.06)*; TK Gristmill Software: Overland Park, KS, USA, 2013.
48. Bader, R.F.W. A Bond Path: A Universal Indicator of Bonded Interactions. *J. Phys. Chem. A* **1998**, *102*, 7314–7323. [[CrossRef](#)]
49. Espinosa, E.; Molins, E.; Lecomte, C. Hydrogen Bond Strengths Revealed by Topological Analyses of Experimentally Observed Electron Densities. *Chem. Phys. Lett.* **1998**, *285*, 170–173. [[CrossRef](#)]
50. Vener, M.V.; Egorova, A.N.; Churakov, A.V.; Tsirelson, V.G. Intermolecular Hydrogen Bond Energies in Crystals Evaluated Using Electron Density Properties: DFT Computations with Periodic Boundary Conditions. *J. Comput. Chem.* **2012**, *33*, 2303–2309. [[CrossRef](#)]

51. Domínguez-Martín, A.; Brandi-Blanco, M.P.; Matilla-Hernández, A.; El Bakkali, H.; Nurchi, V.M.; González-Pérez, J.M.; Castiñeiras, A.; Niclós-Gutiérrez, J. Unraveling the Versatile Metal Binding Modes of Adenine: Looking at Molecular Recognition Patterns of Deaza- and Aza-adenines in Mixed Ligand Metal Complexes. *Coord. Chem. Rev.* **2013**, *257*, 2814–2838.
52. Vílchez-Rodríguez, E.; Pérez-Toro, I.; Bauzá, A.; Matilla-Hernández, A. Structural and Theoretical Evidence of the Depleted Proton Affinity of the N3-Atom in Acyclovir. *Crystals* **2016**, *6*, 193.
53. Pérez-Toro, I.; Domínguez-Martín, A.; Choquesillo-Lazarte, D.; Vílchez-Rodríguez, E.; González-Pérez, J.M.; Castiñeiras, A.; Niclós-Gutiérrez, J. Lights and Shadows in the Challenge of Binding acyclovir, a synthetic Purine-like Nucleoside with Antiviral Activity, at an Apical-Distal Coordination Site in Copper-Polyamine Chelates. *J. Inorg. Biochem.* **2015**, *148*, 84–92. [[CrossRef](#)]
54. Pérez-Toro, I.; Domínguez-Martín, A.; Choquesillo-Lazarte, D.; González-Pérez, J.M.; Castiñeiras, A.; Niclós-Gutiérrez, J. Highest Reported Denticity of a Synthetic Nucleoside in the Unprecedented Tetradentate Mode of Acyclovir. *Cryst. Growth Des.* **2018**, *18*, 4282–4286. [[CrossRef](#)]
55. Bats, J.W.; Nasiri, H.R. CSD Database, reference code NULCO. Private Communication, 2015.
56. Atria, A.M.; Corsini, G.; Herrera, N.; Garland, M.T.; Baggio, R. Two Isomorphous Transition Metal Complexes Containing a Protonated Diaminopurine Ligand: Diaquabis(2,6-diamino-7H-purin-1-ium- κN^9) bis(homophthalato- κO)nickel(II) Tetrahydrate and the Cobalt(II) Analogue. *Acta Crystallogr.* **2011**, *67*, m169–m172. [[CrossRef](#)]
57. Atria, A.M.; Garland, M.T.; Baggio, R. 2,6-Diamino-9H-purine Monohydrate and Bis(2,6-diamino-9H-purin-1-ium) 2-(2-Carboxylatophenyl)acetate Heptahydrate: Two Simple Structures with Very Complex Hydrogen-bonding Schemes. *Acta Crystallogr.* **2010**, *66*, o547–o552. [[CrossRef](#)]
58. Belletire, J.L.; Schneider, S.; Shackelford, S.A.; Peryshkov, D.V.; Strauss, S.H. Pairing Heterocyclic Cations with closo-Dodecafluorododecaborate(-). Synthesis of Binary Heterocyclium(1+) Salts and $\text{Ag}_4(\text{heterocycle})_8^{4+}$ Salt of $\text{B}_{11}\text{F}_{12}^{2-}$. *J. Fluor. Chem.* **2011**, *132*, 925–936. [[CrossRef](#)]
59. Yang, E.-C.; Chan, Y.-N.; Liu, H.; Wang, Z.-C.; Zhao, X.J. Unusual Polymeric $\text{Zn}^{\text{II}}/\text{Cd}^{\text{II}}$ Complexes with 2,6-Diaminopurine by Synergistic Coordination of Nucleobases and Polycarboxylate Anions: Binding Behavior, Self-Assembled Pattern of the Nucleobase, and Luminescent Properties. *Cryst. Growth Des.* **2009**, *9*, 4933–4944. [[CrossRef](#)]
60. Liu, Z.-Y.; Dong, H.-M.; Wang, X.G.; Zhao, X.-J.; Yang, E.-C. Three Purine Containing Metal Complexes with Discrete Binuclear and Polymeric Chain Motifs: Synthesis, Crystal Structure and Luminescence. *Inorg. Chim. Acta* **2014**, *416*, 135–141. [[CrossRef](#)]
61. Atria, A.M.; Parada, J.; Moreno, Y.; Suárez, S.; Baggio, R.; Peña, O. Synthesis, Crystal Structure and Magnetic Properties of Diaquabis(2,6-diamino-7H-purin-1-ium- κN^9)bis(4,4'-oxydibenzoato- κO)cobalt(II) Dihydrate. *Acta Crystallogr.* **2018**, *74*, 37–44.
62. Atria, A.M.; Morel, M.; Garland, M.T.; Baggio, R. Bis(2,6-diamino-1H-purin-3-ium) Di- μ -croconato- $\kappa^3\text{O},\text{O}':\text{O}'';\kappa^3\text{O}:\text{O}',\text{O}''$ -bis[tetraaqua(croconato- $\kappa^2\text{O},\text{O}'$)-neodymium(III)]. *Acta Crystallogr.* **2011**, *67*, m17–m21. [[CrossRef](#)]
63. Atria, A.M.; Garland, M.T.; Baggio, R. Tetraaquabis(2,6-diamine-7H- κN^9)cobalt(II) benzene-1,2,4,5-tetracarboxylate tetrahydrate. *Acta Crystallogr.* **2011**, *67*, m275–m278. [[CrossRef](#)]

